

Linear and nonlinear optical properties of Au–polymer metallodielectric Bragg stacks

Tammy K. Lee,* Alan D. Bristow,[†] Jens Hübner, and Henry M. van Driel

Department of Physics and Institute for Optical Sciences, University of Toronto, 60 St. George Street, Toronto, Ontario M5S 1A7, Canada

Received February 17, 2006; revised June 21, 2006; accepted July 14, 2006; posted July 18, 2006 (Doc. ID 68075)

We demonstrate the fabrication of one-dimensional metallodielectric Bragg stacks (MDBSs) from 500 nm spin-coated poly(methyl methacrylate) and 20 nm evaporated Au layers; one-, two-, and three-bilayer structures are achieved with good homogeneity (<2% thickness variation). The linear reflection and transmission spectra show very strong modulation relative to the constituent materials for only a few bilayers; transmission windows associated with sharp Bragg resonances are observed at ~ 600 and ~ 850 nm, while other regions provide reflections of >90%. Nonlinear absorption was measured by a z -scan technique and is observed to be enhanced at the Bragg resonances. The ~ 600 nm peak of the three-bilayer MDBS is enhanced by approximately seven times compared to a single Au film. The wavelength dependence of the nonlinear enhancement can be correlated with the attenuation parameter. The experimental results are in good agreement with numerical simulations based on a transfer-matrix method employing the known physical and optical parameters. The MDBSs show strong potential as versatile and inexpensive components for optical devices. © 2006 Optical Society of America

OCIS codes: 230.1480, 160.3900, 190.4400.

1. INTRODUCTION

While metals have found extensive use for controlling electromagnetic radiation in the microwave region of the spectrum,^{1,2} their application in the infrared and visible regions has largely been restricted to mirrors. However, metal films with thicknesses of the order of their skin depth (typically tens of nanometers)³ are optically transparent, and have recently been incorporated into various types of photonic devices. By periodically spacing ultrathin metal films into metallodielectric Bragg stacks (MDBSs)^{4,5} the transmission and/or reflection can be enhanced.⁶ The large refractive index contrast between the dielectric and metal layers of a MDBS results in structures that require only a few periods (bilayers) to obtain strong modulation of the linear optical spectra. These MDBSs can also enhance the already large nonlinear optical properties of the single metal layers.

Much experimental research has been performed on films of metal nanoparticles in colloidal suspension^{7–10} to obtain enhanced optical properties. However, the fabrication requires complex chemistry to obtain the nanoparticles that often suffer from poor monodispersity. In ultrathin metal films, clustering can occur to create self-assembled nanometer-sized granules.¹¹ Above a certain film thickness, percolation occurs and the layer becomes more homogeneous. These plane ultrathin metal films have been incorporated into MDBSs with SiO₂ layers as the dielectric medium.¹² However, the SiO₂ layers are produced by complicated deposition techniques. In this paper, we present Au/polymer MDBSs that were fabricated by evaporation of Au layers and spin coating of polymer layers; this method allows for the easy and inexpensive assembly of MDBSs.

Through linear reflection, transmission, and nonlinear

z -scan measurements, we demonstrate that the one-, two-, and three-bilayer structures show very little surface roughness, have strongly modified linear spectra (compared to the constituents), and enhance the nonlinear absorption close to Bragg resonances. In the rapidly advancing field of photonics, the need for high-quality materials that are easy to fabricate is very important for both linear and nonlinear applications. MDBSs can be designed to have the Bragg resonances at wavelengths that are useful for applications where Au is normally highly reflective, e.g., in telecommunications bands and in the range where Ti:sapphire lasers operate. Furthermore, the polymer dielectric layer can be mixed with dyes, quantum dots, or other optically active materials to provide tunable emission.¹³

2. EXPERIMENTAL

The MDBSs were fabricated on commercially available, 6-mm thick BK7 substrates. Each bilayer consists of a gold (99.99% Au) layer and a poly(methyl methacrylate) (PMMA) layer; the target layer thicknesses were ~ 20 and ~ 500 nm, respectively. For the first bilayer, the Au was evaporated directly onto the substrate surface followed by the spin-coated polymer. The two- and three-bilayer samples were produced by the subsequent addition of Au/polymer bilayers to the existing structure. Figure 1(a) shows a schematic of the three-bilayer MDBS.

Evaporation of the Au layers took place in a 10^{-5} Torr vacuum with a 1.8 A current passing through a tungsten crucible holding the Au nugget. The evaporation rate was approximately 0.05 nm/s to ensure good layer uniformity. The Au layers have a mean roughness of 15 Å, estimated by atomic force microscopy [shown in Fig. 2(a)], and an

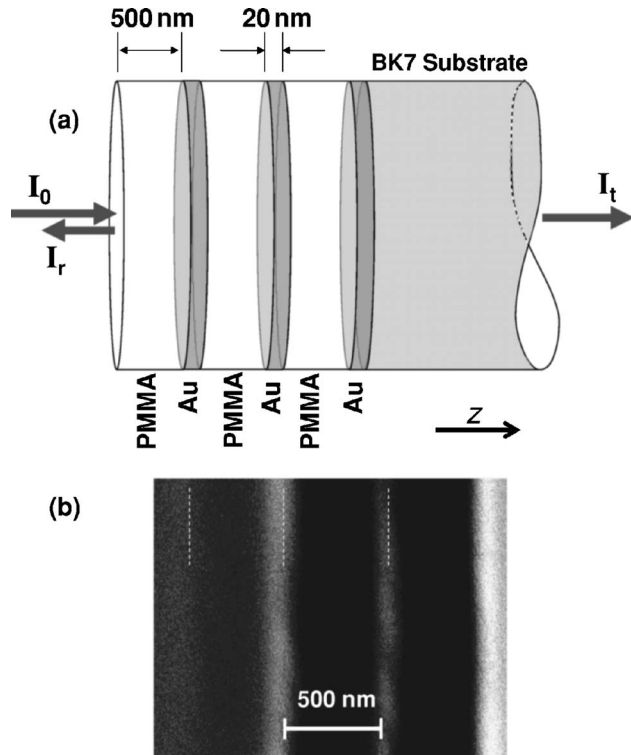


Fig. 1. (a) Schematic of the three bilayer Au/PMMA metallodielectric Bragg stack; also illustrated are the experimental geometries. (b) Cross section scanning electron micrograph of the three-bilayer Bragg stack.

average thickness of 24 ± 2 nm, determined by ellipsometry and profilometry. Note that for ellipsometry, the rear surface of the substrate was frosted to avoid specular reflections that would otherwise reduce the accuracy of the measurement. Prior to the fabrication of the structures, the spin-coating process was optimized to obtain the correct PMMA thickness by varying the polymer concentration and spin speed. Figure 2(b) shows the ellipsometry (dashed curves) and profilometry (solid curves) results of the polymer thickness obtained as a function of spin speed for two concentrations of the PMMA solution. It was found that a target thickness of ~ 500 nm for each layer produced the best surface homogeneity. This was achieved by spinning a 0.5 ml droplet of 5.9 wt. % PMMA at 1000 rpm, yielding average layer thicknesses of 483 ± 50 nm.

A cross-section scanning electron microscope image of the three-bilayer MDBS is shown in Fig. 1(b). The sample was canted over at 80° so that the surface is still slightly visible in the image. From left to right, the dashed white lines indicate the top of the MDBS and the three Au layers. The image is blurred because of fast surface charging of the structure, which is due to the poor mobility in the polymer layers and BK7 substrate. This implies that the layer quality is significantly better than that which can be estimated from Fig. 1(b). It is therefore difficult to obtain accurate values of the layer thicknesses or the surface and interfacial roughness from this technique. Nonetheless, it is expected that the interfacial roughness of the MDBSs grows with the increasing number of layers; this

disorder is discussed later in terms of the optical experiments, which are more appropriate for these measurements.

Linear reflection and transmission spectroscopy were performed on the MDBSs using collimated and linearly polarized light from a tungsten-halogen lamp. The samples were mounted in either reflection or transmission geometry and illuminated at near-normal incidence ($< 1^\circ$), as illustrated in Fig. 1. Index-matching fluid and a microscope slide were used to make the frosted rear surface of the substrate optically flat during the transmission measurements. The transmitted light was analyzed by a 25 cm spectrometer with a dual-Si/InGaAs detector attached. It should be noted that the different sensitivities of the two regions of the detector lead to discontinuities in the parts of the spectra where the wavelengths overlap.

Nonlinear z -scan measurements were performed using an amplified laser system operating at a 1 kHz repetition rate, which pumps an optical parametric amplifier to obtain 200 fs infrared pulses. These pulses were frequency doubled in a 1 mm thick β -barium borate (BBO) crystal to generate wavelengths between 550 and 650 nm. The beam was spatially filtered and focused by a 10 cm focal

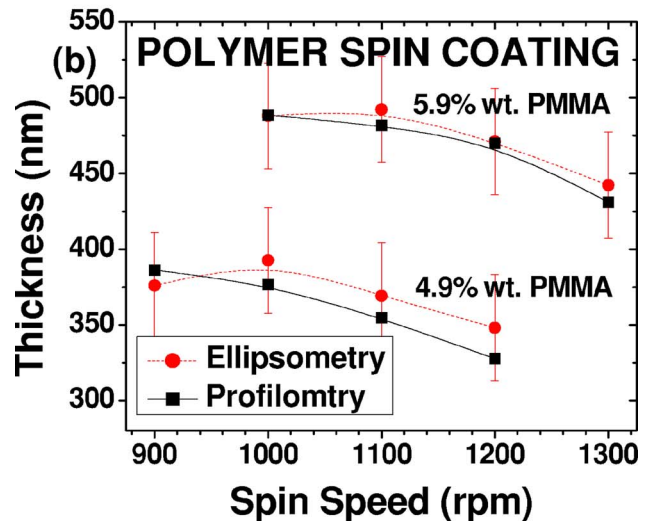
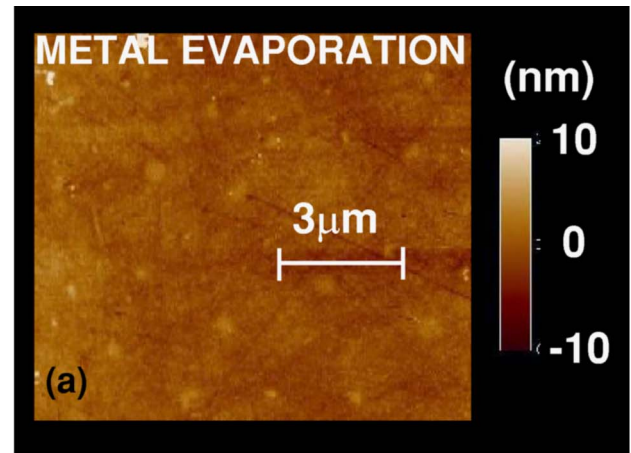


Fig. 2. (Color online) (a) Atomic force micrograph of the surface of a single Au film. (b) Ellipsometry and profilometry data for the PMMA thickness as a function of spin speed for two concentrations.

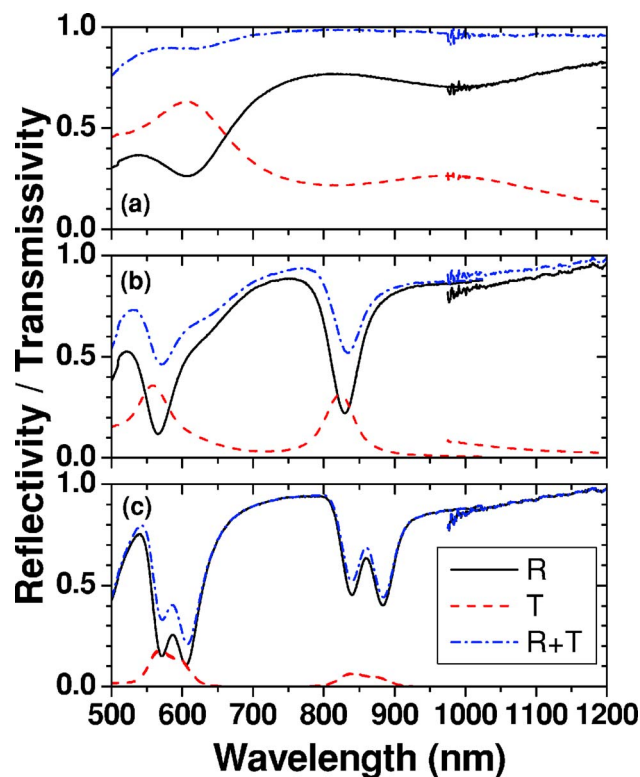


Fig. 3. (Color online) Experimental reflectivity (R), transmissivity (T), and $R+T$ spectra for the (a) one-bilayer, (b) two-bilayer, and (c) three-bilayer MDBSs.

length lens to a $1/e$ spot diameter of $70\ \mu\text{m}$ with a Rayleigh range of approximately $6.5\ \text{mm}$. Individual samples were mounted in the beam path, on an automated translation stage that scans through the focus over a distance of $-50 \leq z \leq 50\ \text{mm}$. To optimize the signal-to-noise ratio and reduce the laser amplitude fluctuations, a balance detection scheme was used; the light transmitted through the sample was collimated onto one of the photodiodes and referenced against a portion of the input beam.

3. RESULTS AND DISCUSSION

A. Linear Properties

For a pure metal film to be optically transparent it needs to be less than a few tens of nanometers thick; red and infrared light are almost completely reflected by a $60\ \text{nm}$ thick Au film. Moreover, absorption in thin Au films is negligible for light at these wavelengths, although the imaginary part of the refractive index, κ , is large but decreases toward a shorter wavelength. At wavelengths of $<600\ \text{nm}$, the real part of the refractive index (n) increases while κ remains significantly large for absorption to occur. The Au film does not behave like a free electron metal since d -band electrons permit interband transitions for wavelengths below $\sim 600\ \text{nm}$. For a $\sim 20\ \text{nm}$ thick Au film, the optical properties described are nearly identical to the one-bilayer structure characterized experimentally; see Fig. 3(a), which summarizes the reflection (R), transmission (T), and the $R+T$ data. One slight variation observed here is weak Fabry–Pérot interference introduced by the polymer layer, discernible as a slight dip in the reflectivity (and peak in the transmissivity) at approxi-

mately $1\ \mu\text{m}$. Otherwise, the spectra show that in the visible, the absorption is nearly 30%, but that it reduces significantly toward infrared wavelengths where reflection dominates. Pure Au films of this thickness have a low damage threshold, making them poor candidates for nonlinear optical applications. The additional polymer layer leaves the optical properties mostly unchanged while protecting the metal with a more robust dielectric surface that can withstand higher intensities.

Figures 3(b) and 3(c) summarize the data for the two and three MDBSs, respectively. In both cases, the optical properties are clearly different from the one-bilayer structure and show more similarity to dielectric Bragg stacks. The periodic spacing of the ultrathin Au layers gives rise to a $>90\%$ reflectivity between 700 and $800\ \text{nm}$. Transmission windows open up at ~ 850 and $\sim 600\ \text{nm}$, which (owing to the sample thickness) correspond to the second- and third-order Bragg resonances, respectively. However, unlike dielectric Bragg stacks, where the indices of the materials are very similar and the layer thicknesses are therefore almost identical, in the MDBSs, the Au layer must be very thin; consequently, neither the Au nor the PMMA layers have thicknesses that satisfy the Bragg condition ($\lambda/4$). Nonetheless, the spectra exhibit features that are expected for one-dimensional periodic structures and indeed do so with only a few periods. This makes the high refractive index contrast between the constituent materials advantageous, especially when compared to AlAs/GaAs Bragg stacks that require approximately 15 bilayers for high reflectivity.¹⁴

Transfer-matrix calculations were employed to fit the experimental spectra using parameters that were based

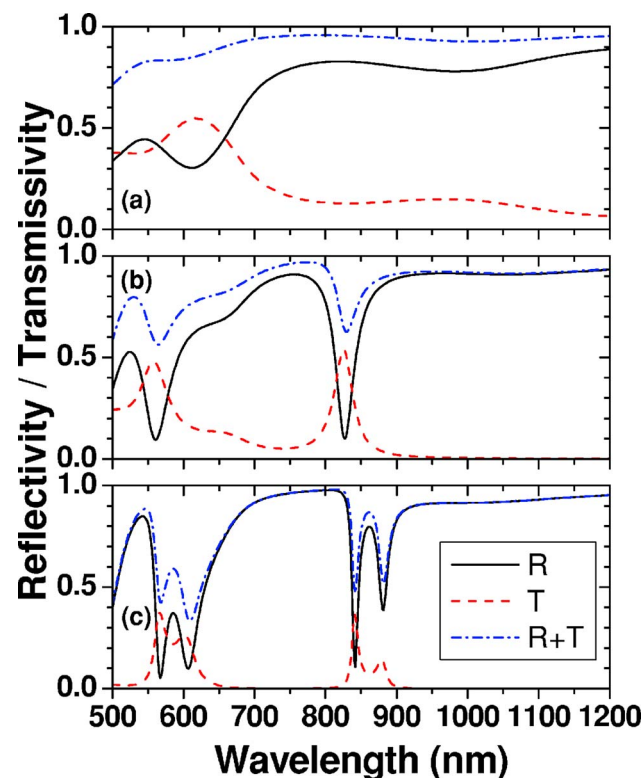


Fig. 4. (Color online) Theoretical R , T , and $R+T$ spectra for the (a) one-bilayer, (b) two-bilayer, and (c) three-bilayer MDBSs.

upon the measured layer thicknesses and indices. The ellipsometry technique yielded the complex refractive index of the polymer ($n=1.47, \kappa=0$), which is assumed to be wavelength independent in the spectral region of interest. The dispersions for Au available in the literature^{15,16} vary significantly, and the choice alters the quality of the fit. Here, the Johnson and Christy¹⁶ values for n and κ were used in modeling the reflectivity and transmissivity spectra. Figure 4 shows the simulated R , T , and $R+T$ spectra for each of the three structures. The thicknesses obtained from the fitting are 30 nm for the first Au layer and 526 nm for the first polymer layer, describing the one-bilayer structure in Fig. 4(a); 30 and 522 nm for the second Au and PMMA layers, yielding the two-bilayer structure in Fig. 4(b); and 27 and 503 nm for the third Au and PMMA layers, giving the three-layer structure in Fig. 4(c). For all three MDBSs, the numerical simulations reproduce all the key features observed experimentally; however, the Bragg resonances are slightly narrower than those seen in Fig. 3. Therefore, it can be estimated that the variation in the structures' thicknesses is of the order of 2%, averaged over the area of the incident beam diameter (~ 2 mm). This value grows slightly with the increasing number of bilayers, resulting in a trade-off between the incoherent scattering of each additional bilayer and the improved strong Bragg scattering due to the total number of bilayers. From this, an upper limit to the number of useful bilayers can be determined.

Since a MDBS cannot be $\lambda/4$ matched, the observed Bragg resonances are relatively sharp in comparison to those observed for dielectric Bragg stacks, which typically appear as Fabry–Perot oscillations on either side of the stop band. For the MDBSs, the resonances occur when constructive interference allows the radiation to be enhanced in the forward direction in each successive ultrathin Au film. The large disparity between the layer thicknesses means that this condition can only be met over very narrow regions of the spectrum (accounting for the sharp resonance), compared to strong reflection that occurs over a wider region. When this occurs, the forward enhancement is related to the κ of the Au films, since the real part of the refractive index is comparatively low at the wavelengths where the resonances occur. In numerical simulations where the value of κ is artificially reduced, the Bragg resonances flatten out and the spectra become more reflective over the entire region.

Numerical simulations were also performed for wavelengths longer than 1200 nm, revealing the first-order Bragg resonances at ~ 1600 nm. This wavelength corresponds to the telecom–datacom L band, where Au is normally highly reflective. Owing to the thickness of the fabricated structure, the experimental results only show the second- and third-order resonances at ~ 850 and 600 nm, respectively. The higher-order resonances have the advantage of a narrower spectral width but are less sensitive to refractive index changes compared to the first-order resonance.

B. Nonlinear Properties

Open aperture z -scan experiments are sensitive to intensity-dependent absorption effects, $\beta_{\text{eff}}I_0$, where I_0 is the peak intensity and β_{eff} is the effective nonlinear ab-

sorption coefficient. Note that closed aperture z scans that measure the intensity-dependent contribution to the refractive index are not performed because nonlinear refraction is negligible for the MDBSs. This is due to the small layer thickness and the experimental conditions. Furthermore, since the PMMA film shows no nonlinear absorption, the nonlinearity for each Bragg stack can only be compared to the open-aperture z -scan measurements performed on a single Au film of the same thickness. The nonlinear response of an Au metal film is dominated by Fermi smearing,^{17,18} a fast thermal process where the electrons are heated to a temperature (>1000 K) much higher than that of the ionic lattice. The d band to conduction-band excitation is pulse-width limited, but electron relaxation that occurs through electron–phonon interactions, takes place on a several picosecond time scale. This fast thermal redistribution in the single and incorporated Au films alters the absorption coefficient, making it effectively intensity dependent. This nonlinear absorption process cannot be directly related to two-photon absorption [related to an $\text{Im}(\chi^3)$] as is sometimes casually done in the literature. Also, since the open aperture z -scan measurement is a one-beam technique, the pulse width of the laser is important for obtaining absolute values of the nonlinearity.

Figure 5 shows the z -scan traces for the single Au film and the three Bragg structures. These scans are obtained at normal incidence for 600 nm with an incident peak power of 1.55 MW, where the intensity varies over the scan range giving 40 GW/cm^2 at the focus of the beam. The traces are normalized by subtracting and dividing a low-power (50 kW) trace to remove any unwanted offsets. From Fig. 5 it can be seen that the depth of the differential transmission is $|\Delta T/T|=4\%$ for the single Au film, from which the effective nonlinear absorption coefficient can be determined using the standard analysis for open aperture z scans¹⁹; this yields a value of $\beta_{\text{eff}}=1.2 \times 10^{-5} \text{ cm/W}$, which is approximately 2 orders of magnitude smaller than the value obtained by Smith *et al.*¹¹ Their experiments, however, were performed with pulse widths of 30 ps. The discrepancy likely reflects the differ-

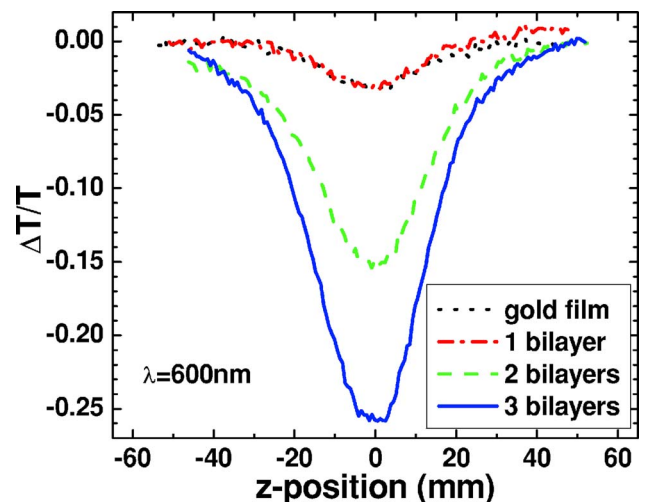


Fig. 5. (Color online) Typical experimental z -scan traces for the Au film and the one-, two-, and three-bilayer MDBSs at $\lambda = 600$ nm with 1.55 MW peak power.

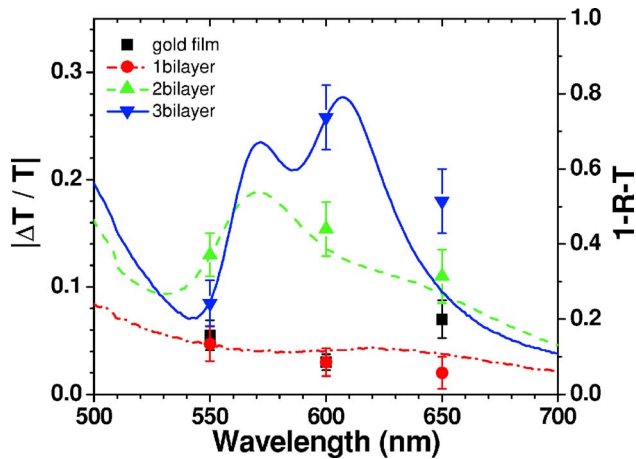


Fig. 6. (Color online) Maximum experimental values of $|\Delta T/T|$ versus wavelength for the single Au film and the one-, two-, and three-bilayer MDBSs. Also plotted (solid or dashed curves) are the $1-R-T$ linear experimental spectra for all three MDBSs.

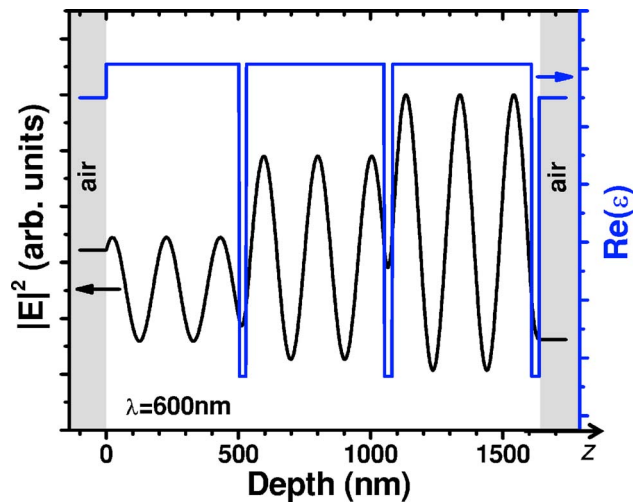


Fig. 7. (Color online) Distribution of the square of the electric field amplitude within the three-bilayer MDBS at $\lambda=600$ nm, shown along with the profile of the real part of the dielectric constant.

ence in electron peak temperature and temporal evolution of the excitation during the different optical pulse widths. Our preliminary studies reveal that the effective nonlinearity does indeed increase when we stretch the pulse width by a factor of 2.

Figure 5 also shows that for the same incident intensity, the differential transmission increases as the number of bilayers goes up; $|\Delta T/T|$ is 4%, 17%, and 26% for the one-, two-, and three-bilayer structures, respectively. For the three-bilayer structure, this corresponds to an enhancement of the β_{eff} by $\sim 7\times$ with respect to the single Au film. In general, the enhancement of the effective nonlinearity relates to the strength of the Bragg resonance and can be mapped onto the attenuation parameter ($1-R-T$). In Fig. 6, the differential transmission values are plotted for the single Au film and all three Bragg structures at 550, 600, and 650 nm; also shown are the ($1-R-T$) spectra determined from the linear optical measurements. The correlation between $|\Delta T/T|$ and ($1-R-T$) is

very good, confirming that the enhancement is, in fact, related to the attenuation parameter. Moreover, the values of differential transmission observed here for the Au/PMMA are comparable to those observed previously in the five bilayer Cu/SiO₂ structures.¹² This is partly due to the stronger *d* band to conduction-band transition expected in Au as compared to Cu.²⁰ However, it should be noted that in these experiments, the Au layers are slightly thicker than the Cu layers, and that we probe the third-order Bragg resonance, whereas Lepeshkin *et al.* probe the fundamental resonance.

The electric field $\mathbf{E}(z)$ profile in the Bragg structures can be determined by integrating Maxwell's equations as a function of depth in the structure, assuming plane waves that are propagating at normal incidence to the layer interfaces. The linear and nonlinear optical coefficients can contribute to the forward transmission, such that⁶:

$$\frac{d\mathbf{E}(z)}{dz} = ik\mathbf{H}, \quad (1)$$

$$\frac{d\mathbf{H}(z)}{dz} = ik \left[\epsilon(z) + \frac{n^2 \epsilon_0 \lambda \beta_{\text{eff}}}{2\pi} |\mathbf{E}(z)|^2 \right] \mathbf{E}, \quad (2)$$

where $k=2\pi/\lambda$, λ is the wavelength, and the linear and nonlinear coefficients n and β_{eff} were determined previously. The square of the electric field is plotted as a function of depth in Fig. 7 for 600 nm light propagating through the three-bilayer MDBS. The figure shows that the strength of $|\mathbf{E}(z)|^2$ increases in each successive region of PMMA, with field nodes overlapping the Au layers. The radiation constructively interferes to produce enhancements in the forward direction. Consequently, the intensity-dependent absorption at the exit face of the sample can be calculated, allowing for the open-aperture z -scan data to be reproduced; the $|\mathbf{E}(z)|^2$ profiles and, consequently, $|\Delta T/T|$ traces were simulated for the other samples and wavelengths to confirm the properties observed in Fig. 6. For the three-bilayer structure in particular, enhancements in the nonlinear properties are shown close to the Bragg resonance, whereas no enhancement is observed far off resonance at 700 nm.

4. CONCLUSIONS

We have fabricated high-quality metallodielectric Bragg stacks via simple techniques, namely, by alternating ~ 20 nm evaporated Au and ~ 500 nm spin-coated PMMA layers. One-, two-, and three-bilayer structures have been created with typical interfacial homogeneity of $\sim 2\%$. The structures were characterized in terms of their linear optical properties. Bragg resonances were observed at ~ 850 and ~ 600 nm, while at other wavelengths, regions of high reflectivity ($>90\%$) were seen. The optical properties of the structures are strongly modified from those of the constituent materials and demonstrate the advantage of the high refractive index contrast with only a few bilayers. All linear results were verified by transfer-matrix calculations.

The nonlinear transmission properties were studied close to the 600 nm resonance and compared to a single

~25 nm Au film. For the three-bilayer structure, there is a seven times enhancement of the nonlinear absorption coefficient close to the peak of the resonance; in general the enhancement follows the attenuation parameter ($1 - R - T$) that was measured by linear spectroscopy. The enhancement and the shape of the resonances were numerically simulated by integrating Maxwell's equations as a function of depth in the structure. The simulation results are able to reproduce the main features of the experiments. The metallodielectric Bragg stacks are a demonstration of inexpensive fabrication and show great potential as versatile components for both linear and nonlinear optical devices.

ACKNOWLEDGMENTS

We thank Eugenia Kumacheva and Chantal Paquet for assistance with the material fabrication and we also thank John E. Sipe and Jarkko J. Saarinen for stimulating discussions. This work is funded by the Natural Sciences and Engineering Research Council of Canada and Photonics Research Ontario.

The corresponding author is A. D. Bristow, whose e-mail address is alan.bristow@utoronto.ca.

*Present address, the Institute of Optics, University of Rochester, Rochester, New York, 14627-0186.

†Present address, the Institute for Solid State Physics, University of Hannover, 30167 Hannover, Germany.

REFERENCES

1. D. R. Smith, S. Schultz, N. Kroll, M. Sigalas, K. M. Ho, and C. M. Soukoulis, "Experimental and theoretical results for a two-dimensional metal photonic band-gap cavity," *Appl. Phys. Lett.* **65**, 645–647 (1994).
2. D. F. Sievenpiper, M. E. Sickmiller, and E. Yablonovitch, "3D wire mesh photonic crystals," *Phys. Rev. Lett.* **76**, 2480–2483 (1996).
3. D. E. Aspnes, "Optical properties of thin films," *Thin Solid Films* **89**, 249–262 (1982).
4. M. J. Bloemer and M. Scalora, "Transmissive properties of Ag/MgF₂ photonic band gaps," *Appl. Phys. Lett.* **72**, 1676–1678 (1998).
5. M. Scalora, M. J. Bloemer, A. S. Pethel, J. P. Dowling, C. M. Bowden, and A. S. Manka, "Transparent, metallo-dielectric, one-dimensional, photonic band-gap structures," *J. Appl. Phys.* **83**, 2377–2383 (1998).
6. R. S. Bennink, Y.-K. Yoon, R. W. Boyd, and J. E. Sipe, "Accessing the optical nonlinearity of metals with metal-dielectric photonic bandgap structures," *Opt. Lett.* **24**, 1416–1418 (1999).
7. R. D. Averitt, S. L. Westcott, and N. J. Halas, "Ultrafast electron dynamics in gold nanoshells," *Phys. Rev. B* **58**, 10203(R)–10206(R) (1998).
8. S. Link and M. A. El-Sayed, "Spectral properties and relaxation dynamics of surface plasmon electronic oscillations in gold and silver nanodots and nanorods," *J. Phys. Chem. B* **103**, 8410–8426 (1999).
9. H. Li and E. Kumacheva, "Core-shell particles with conductive polymer cores," *Colloid Polym. Sci.* **281**, 1–9 (2003).
10. K. P. Velikov, W. L. Vos, A. Moroz, and A. van Blaaderen, "Reflectivity of metallodielectric photonic glasses," *Phys. Rev. B* **69**, 075108 (2004).
11. D. D. Smith, Y. Yoon, R. W. Boyd, J. K. Campbell, L. A. Baker, R. M. Crooks, and M. George, "z-scan measurement of the nonlinear absorption of a thin gold film," *J. Appl. Phys.* **86**, 6200–6205 (1999).
12. N. N. Lepeshkin, A. Schweinsberg, G. Piredda, R. S. Bennink, and R. W. Boyd, "Enhanced nonlinear optical response of one-dimensional metal-dielectric photonic crystals," *Phys. Rev. Lett.* **93**, 123902 (2004).
13. Y. Liu, F. Mahdavi, and S. Blair, "Enhanced fluorescence transduction properties of metallic nanocavity arrays," *IEEE J. Sel. Top. Quantum Electron.* **11**, 778–784 (2005).
14. M. K. Emsley, O. Dosunmu, and M. S. Ünlü, "Silicon substrates with buried distributed Bragg reflectors for resonant cavity-enhanced optoelectronics," *IEEE J. Sel. Top. Quantum Electron.* **8**, 948–955 (2002).
15. E. D. Palik, ed., *Handbook of Optical Constants in Solids* (Academic, 1985).
16. P. B. Johnson and R. W. Christy, "Optical constants of noble metals," *Phys. Rev. B* **6**, 4370–4379 (1972).
17. R. H. M. Groeneveld, R. Sprik, and A. Lagendijk, "Femtosecond spectroscopy of electron-electron and electron-phonon energy relaxation in Ag and Au," *Phys. Rev. B* **51**, 11433–11445 (1995).
18. C.-K. Sun, F. Vallée, L. Acioli, E. P. Ippen, and J. G. Fujimoto, "Femtosecond investigation of electron thermalization in gold," *Phys. Rev. B* **48**, 12365–12368 (1993).
19. M. Sheik-Bahae, A. A. Said, T. H. Wei, D. J. Hagan, and E. W. van Stryland, "Sensitive measurement of optical nonlinearities using a single beam," *IEEE J. Quantum Electron.* **26**, 760–769 (1990).
20. M. Suffczynski, "Optical constants of metals," *Phys. Rev.* **117**, 663–671 (1960).